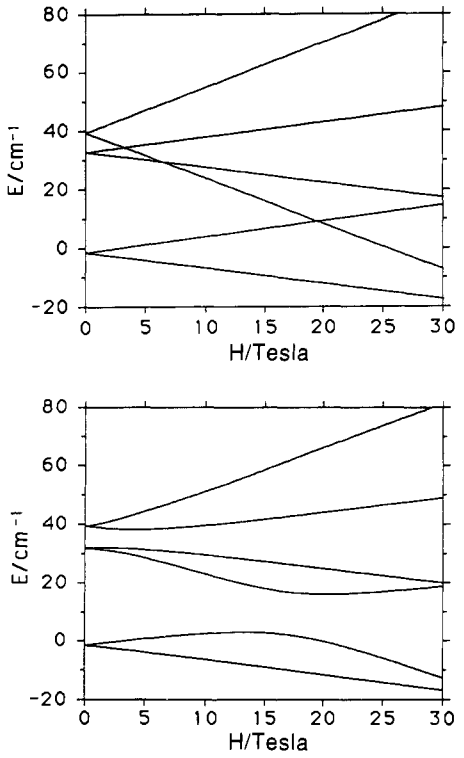

Figure 3. Variation of the low-lying-state energies versus the field H for Cu(salen)Ni(hfa)$_2$: (top) H parallel to the z direction of **D**; (bottom) H perpendicular to the z direction of **D** (see text).

method. The M versus H plots are shown in Figure 2. The sample was extracted in a constant magnetic field between compensated pick-up coils connected in series opposition. The integrated signal of the induced voltage was proportional to M. The continuous magnetic field up to 20 T was produced by a water-cooled Bitter magnet. The calibration and the sensitivity of the apparatus were previously described in detail.[7] The molar magnetization M_u along the direction u of the magnetic field H_u is given by

$$M_u = N[\sum_i(-\partial E_{i,u}/\partial H_u)\exp(-E_{i,u}/kT)]/[\sum_i \exp(-E_{i,u}/kT)] \quad (1)$$

where the $E_{i,u}$'s are the energies of the six levels in the presence of the field. The average molar magnetization is then calculated as[8]

$$M = (4\pi)^{-1}\int_{space} M_{\theta,\phi}\sin\theta\, d\theta\, d\phi \quad (2)$$

The energies $E_{i,u}$ are obtained by diagonalization of the spin Hamiltonian (3) by using the $|S, M_S\rangle$ functions associated with

$$\mathcal{H} = -JS_{Cu}\cdot S_{Ni} + S_{Ni}\cdot\mathbf{D}\cdot S_{Ni} + \beta H\cdot(\mathbf{g}_{Cu}\cdot S_{Cu} + \mathbf{g}_{Ni}\cdot S_{Ni}) \quad (3)$$

the pair states as a basis set, where J is the isotropic interaction parameter, $\mathbf{g}_{Cu}$ and $\mathbf{g}_{Ni}$ are the local Zeeman tensors, and **D** is the nickel(II) local anisotropy tensor. In (3), the ZFS within the quartet pair state is assumed to arise entirely from the nickel(II) local anisotropy. In other words, dipolar and anisotropic interactions are neglected. This assumption does not affect the determination of Δ.

When H is parallel to the z direction of **D**, only the $|^1/_2, \pm^1/_2\rangle$ and $|^3/_2, \pm^1/_2\rangle$ functions with the same M_S couple through **D**, so that M_S remains a good quantum number. On the other hand, when H is perpendicular to the z direction, the $|^1/_2, M_S\rangle$ and $|^3/_2, M_S'\rangle$ functions with $M_S \neq M_S'$ couple as well, and the off-diagonal matrix elements are proportional either to **D** or to $\beta\Delta\mathbf{g}H$ ($\Delta\mathbf{g} = \mathbf{g}_{Cu} - \mathbf{g}_{Ni}$). The most important interaction takes place between $|^1/_2, ^1/_2\rangle$ and $|^3/_2, -^3/_2\rangle$ in the field range where the two levels are close to each other. This mixing between ground doublet and excited quartet pair states through **D** leads to magnetization curves that, even at low temperature, are significantly different from what would be expected for a rigorously pure doublet ground state (e.g. a mononuclear copper(II) compound). In particular, instead of showing a saturation magnetization $M_S = g_{1/2}/2\ \mu_B$, $g_{1/2}$ being the Zeeman factor for the doublet state, the M versus H plot continuously increases when H increases. This situation may be explained as follows: In the absence of **D**, the $|^1/_2, -^1/_2\rangle$ and $|^3/_2, -^3/_2\rangle$ levels would intersect for a field value of $-3J/2\beta g_{1/2}$ (around 40 T), with an abrupt transition in the M versus H plot. Due to the coupling of the pair states through **D**, this transition is much smoother and starts at relatively low field.

To fit the two magnetization curves, we used the J scalar, and the $\mathbf{g}_{Cu}$ and $\mathbf{g}_{Ni}$ tensors as deduced from magnetic susceptibility and EPR data,[9] and we determined the **D** tensor by minimizing R defined as $\sum(M^{obs} - M^{calc})^2/\sum(M^{obs})^2$. The three parameters of the problem are then the axial D ($=3D_{zz}/2$) and rhombic E ($=|D_{xx} - D_{yy}|/2$) local anisotropy parameters as well as the angle θ between the local z axes of the $\mathbf{g}_{Cu}$ and **D** tensors.[10] The lowest R value ($=8\times10^{-6}$) was obtained for $D = 12.5$ cm^{-1}, $E/D = 0.06$, and $\theta = 67°$. The ZFS splitting Δ ($=2(D^2 + 3E^2)^{1/2}/3$) within the quartet state of the $Cu^{II}Ni^{II}$ pair is then equal to 8.4 cm^{-1}. The variations of the low-lying-state energies versus the field for both H parallel and perpendicular to the z direction of **D** are shown in Figure 3. This figure emphasizes the mixing of the $|S, M_S\rangle$ functions in the perpendicular case. This is particularly true for $|^1/_2, ^1/_2\rangle$ and $|^3/_2, -^3/_2\rangle$. At very high field, $|^1/_2, ^1/_2\rangle$ becomes $|^1/_2, -^3/_2\rangle$ and $|^3/_2, -^3/_2\rangle$ becomes $|^3/_2, ^1/_2\rangle$. Although this is not the main goal of this communication, it worth mentioning that the large nickel(II) local anisotropy explains why the triplet state for the $[CuNi]_2$ entity is significantly split in zero field. Indeed, the magnitude of this splitting detected in the EPR spectrum is expected to vary as D/J on the one hand and as the interpair interaction J_{AB} on the other hand.[3]

To conclude, very high field magnetization data at low temperatures have provided a quantitative piece of information on the spectrum of the low-lying states that has been impossible to deduce from any other technique. This approach is an important new step in the field of the molecular magnetism.

Registry No. Cu(salen)Ni(hfa)$_2$, 71073-29-5.

(7) Picoche, J. C.; Guillot, M.; Marchand, A. *Physica B* **1989**, *155*, 407.
(8) Day, E. P.; Kent, T. A.; Lindahl, P. A.; Münck, E.; Orme-Johnson, W. H.; Roder, H.; Roy, A. *Biophys. J.* **1987**, *52*, 837.
(9) $J = -23.6$ cm^{-1}; $g_z = 2.24$ is along the direction perpendicular to the copper basal plane, and g_x and $g_y = 2.025$ are in the basal plane; $\mathbf{g}_{Ni}$ is isotropic with the principal value $g_{Ni} = 2.26$.
(10) Due to the weak rhombicity of **D**, the relative orientations of D_{xx} and D_{yy} with respect to the principal directions of $\mathbf{g}_{Cu}$ do not play any role.

Laboratoire de Chimie Inorganique
URA No. 420
Université de Paris-Sud
91405 Orsay, France

Pierre Bergerat
Olivier Kahn*

Service National des Champs Intenses
UPR No. 5021, CNRS
38042 Grenoble, France

Maurice Guillot

Received August 9, 1990

Synthesis and Structural Characterization of $[Hg_7Se_{10}]^{4-}$ and $[Hg_7Se_9]_n^{4n-}$: Novel Metal–Chalcogenide Frameworks

In our investigation of the coordination chemistry of Q_x^{2-} (Q = Se, Te) ligands we have used late transition metals and relatively long polychalcogenide ligands in $M{:}Q_x^{2-}$ ($x = 4, 5$) ratios of 1:2 and 1:3.[1] This combination of reagents usually yields mononuclear

0020-1669/91/1330-1966$02.50/0 © 1991 American Chemical Society

and sometimes binuclear products. Such examples are the mercury polyselenides $[Hg(Se_4)_2]^{2-}$ and $[Hg_2(Se_4)_3]^{2-}$.[1a] On the contrary, a $M:Q_x^{2-}$ ratio of 1:1 yields insoluble polymeric products regardless of x. With Hg^{2+}, for example, $HgSe_4$ and HgSe can be made.[3] It also appears that short-chain polychalcogenides favor larger clusters as in the case of Haushalter's $[Hg_4Te_{12}]^{4-}$,[4] which contains Te_2^{2-} and Te_3^{2-} ligands. As we seek to make a connection between molecular and solid-state chemistry and to achieve the synthesis of compounds with intermediate dimensionality at low temperatures, we set out to investigate the Hg^{2+}/Se_x^{2-} system, where x = 1 and 2, in the ratios between 1:2 and 1:1. Thus, we hoped to avoid either the mononuclear $[Hg(Se_x)_2]^{2-}$ or the insoluble three-dimensional $HgSe_x$ systems. Here we report the successful isolation and structural characterization of $[Hg_7Se_{10}]^{4-}$ and $[Hg_7Se_9]_n^{4n-}$, two novel structures with mono- and diselenide ligands.

The reaction between a dimethylformamide (DMF) solution of $HgCl_2$ and Na_2Se_2 in 2:3 mole ratio in the presence of Et_4NBr followed by filtration and dilution with ether afforded a light brown microcrystalline material. Recrystallization of this material from DMF diluted with ether yielded light red rectangular platelets of $(Et_4N)_4[Hg_7Se_{10}]$ (9% yield). A single-crystal X-ray diffraction study[5] reveals that $(Et_4N)_4[Hg_7Se_{10}]$ is composed of $[Hg_7Se_{10}]^{4-}$ (I) anions and noninteracting Et_4N^+ organic cations. The microcrystalline material obtained before recrystallization is a different $(Et_4N)_xHg_ySe_z$ phase, which by energy dispersive spectroscopy (EDS) gives a Hg:Se ratio of 4:7.[6]

As shown in Figure 1A, I is odd shaped and contains four tetrahedral Hg^{2+} and three linear Hg^{2+} metal ions, which are held together by one diselenide and eight monoselenide ligands. Thus, $[Hg_7(Se_2)(Se)_8]^{4-}$ is a more descriptive formulation. I is reasonably described as a cage with handles. The Se(7)–Hg(6)–Se(8) and Se(9)–Hg(7)–Se(10) pseudolinear fragments on either side of the cage are the handles. The central cage is composed of two oppositely placed planar rhombic Hg_2Se_2 units fused with two five-membered and two six-membered rings. A molecular C_2 axis passes through the Hg(5) atom and bisects the diselenide Se(1)–Se(2) bond. Four mercury atoms, Hg(1), Hg(2), Hg(3), and Hg(4), lie in a plane with Hg(5) lying 2.117 Å above it, while Hg(6) and Hg(7) lie 0.546 and 0.828 Å below it, respectively. The dimensions of I are 9.36 × 7.12 × 3.88 Å.

There are four distorted tetrahedral Hg centers and two distorted linear Hg centers in the structure. The fluctuations in Hg–Se bond distances and angles around tetrahedral Hg atoms range from 2.508 (6) to 3.101 (7) Å and from 88.1 (1) to 136.0 (2)°, respectively, indicating severe distortions around the Hg centers. The longest bonds are between the tetrahedral Hg atoms and the diselenide ligand (average 2.80 (2) Å) and between tetrahedral Hg atoms and the Se(4)–Hg(5)–Se(3) linear unit (average 2.99 (8) Å). Although the bond angle around Hg(5) is 178.9 (2)°, the average angle around Hg(6) and Hg(7) is 167 (1)°, considerably smaller than the ideal 180°. The reason for this distortion stems from the weak interactions between $[Hg_7Se_{10}]^{4-}$ clusters through long ternary Hg–Se intercluster bonds. This results in a linear chain of clusters running parallel to the crystallographic (110) direction, as shown in Figure 1B. The Hg–Se distances between the clusters, Hg(6)–Se(9)′ and Hg(7)–Se(7)′, are 3.256 (5) and 3.235 (5) Å, respectively. These

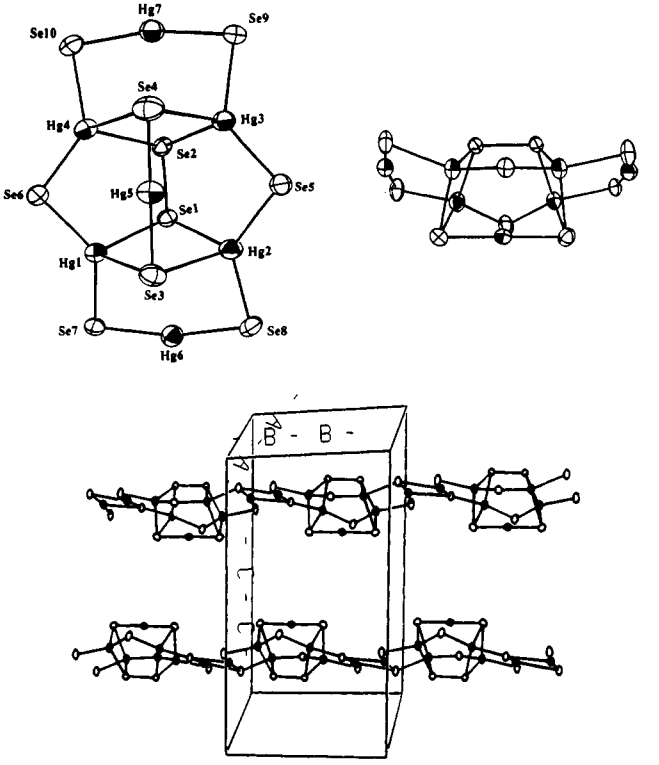

Figure 1. (A) Top: ORTEP representation (two views) and labeling scheme of the structure of the $[Hg_7Se_{10}]^{4-}$ cluster. Selected bond distances (Å) and angles (deg) are as follows: Hg(1)–Se(1), 2.783 (5); Hg(1)–Se(3), 2.919 (5); Hg(1)–Se(6), 2.530 (4), Hg(1)–Se(7), 2.601 (5); Hg(2)–Se(1), 2.819 (4); Hg(2)–Se(3), 3.005 (5); Hg(2)–Se(5), 2.541 (5); Hg(2)–Se(8), 2.587 (5); Hg(3)–Se(2), 2.793 (5); Hg(3)–Se(4), 2.934 (5); Hg(3)–Se(5), 2.531 (4); Hg(3)–Se(9), 2.625 (5); Hg(4)–Se(2), 2.801 (4); Hg(4)–Se(4), 3.101 (7); Hg(4)–Se(6), 2.508 (6); Hg(4)–Se(10), 2.567 (5); Hg(5)–Se(3), 2.411 (5); Hg(5)–Se(4), 2.399 (5); Hg(6)–Se(7), 2.452 (5); Hg(6)–Se(8), 2.443 (6); Hg(7)–Se(9), 2.447 (5); Hg(7)–Se(10), 2.435 (6); Se(1)–Se(2), 2.349 (6); Se(1)–Hg(1)–Se(3), 90.6 (1); Se(1)–Hg(1)–Se(6), 112.8 (2); Se(1)–Hg(1)–Se(7), 99.7 (1); Se(3)–Hg(1)–Se(6), 109.1 (2); Se(3)–Hg(1)–Se(7), 99.0 (1); Se(6)–Hg(1)–Se(7), 136.0 (2); Se(1)–Hg(2)–Se(3), 88.1 (1); Se(1)–Hg(2)–Se(5), 110.8 (1); Se(1)–Hg(2)–Se(8), 106.6 (2); Se(3)–Hg(2)–Se(5), 111.4 (2); Se(3)–Hg(2)–Se(8), 98.3 (2); Se(5)–Hg(2)–Se(8), 132.3 (2); Se(2)–Hg(3)–Se(4), 92.2 (2); Se(2)–Hg(3)–Se(5), 110.4 (2); Se(2)–Hg(3)–Se(9), 98.2 (2); Se(4)–Hg(3)–Se(5), 113.6 (2); Se(4)–Hg(3)–Se(9), 100.3 (1); Se(5)–Hg(3)–Se(9), 133.7 (2); Se(2)–Hg(4)–Se(4), 88.5 (1); Se(2)–Hg(4)–Se(6), 111.5 (2); Se(2)–Hg(4)–Se(10), 102.1 (2); Se(4)–Hg(4)–Se(6), 113.8 (2); Se(4)–Hg(4)–Se(10), 96.3 (2); Se(6)–Hg(4)–Se(10), 134.6 (2); Se(3)–Hg(5)–Se(4), 178.9 (2); Se(7)–Hg(6)–Se(8), 166.0 (2); Se(9)–Hg(7)–Se(10), 168.1 (2). (B) Bottom: One-dimensional mode of interconnecting $[Hg_7Se_{10}]^{4-}$ clusters. Filled circles represent Hg atoms.

distances are shorter than the sum of van der Waals radii of Hg and Se atoms, 3.40 Å, but much longer than normal Hg–Se bonds. There are no Hg–Hg bonds in the cluster. The shortest Hg–Hg distance is 3.440 (3) Å. We note here that there is a structural similarity between the $[Hg_7Se_{10}]^{4-}$ and $[Hg_4Te_{12}]^{4-}$[4] clusters. The former is conceptually derived from the latter by replacement of the Te_3^{2-} handles with two linear Se–Hg–Se units and one μ_4-Te_2^{2-} unit with another linear Se–Hg–Se unit, shown as follows:

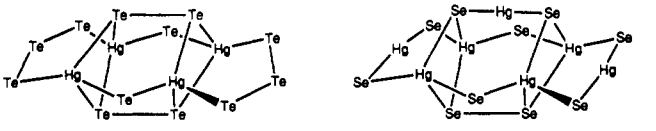

The presence of eight monoselenide ligands in I urged us to use Na_2Se reagent instead of Na_2Se_2, in order to synthesize a compound containing only monoselenide ligands. We recognized that a cluster similar to I could not be stabilized with monoselenides only, since substitution of an Se_2^{2-} for an Se^{2-} would create enough strain in the cage to cause it to adopt a different

(1) (a) Kanatzidis, M. G. *Comments Inorg. Chem.* **1990**, *10*, 161–195. (b) Kanatzidis, M. G.; Huang, S.-P. *Inorg. Chem.* **1989**, *28*, 1513–1514. (c) Kanatzidis, M. G.; Dhingra, S. *Inorg. Chem.* **1989**, *28*, 2024–2026.
(2) (a) Krauter, G.; Weller, F.; Dehnicke, K. *Z. Naturforsch.* **1989**, *44B*, 444–454. (b) Dhingra, S.; Kanatzidis, M. G. Unpublished results.
(3) Kim, K.-W.; Kanatzidis, M. G. Unpublished results.
(4) Haushalter, R. C. *Angew. Chem., Int. Ed. Engl.* **1985**, *24*, 432–433.
(5) Crystal data for $(Et_4N)_4[Hg_7Se_{10}]$ (I): triclinic $P\bar{1}$, Z = 2, a = 12.281 (4) Å, b = 12.555 (6) Å, c = 21.155 (6) Å, α = 96.15 (3)°, β = 98.48 (2)°, γ = 107.84 (3)°, V = 3031 Å^3 at 298 K, and $2\theta_{max}$(Mo Kα) = 43°. Number of data measured: 7413. Number of data having $F_o^2 > 3\sigma(F_o^2)$: 4727. D_{calc} = 2.97 g/cm^3. Crystal dimensions: 0.08 × 0.26 × 0.70 mm. An empirical absorption correction was applied; μ = 236 cm^{-1}. Final R = 0.064 and R_w = 0.075.
(6) Work is in progress to characterize this compound.

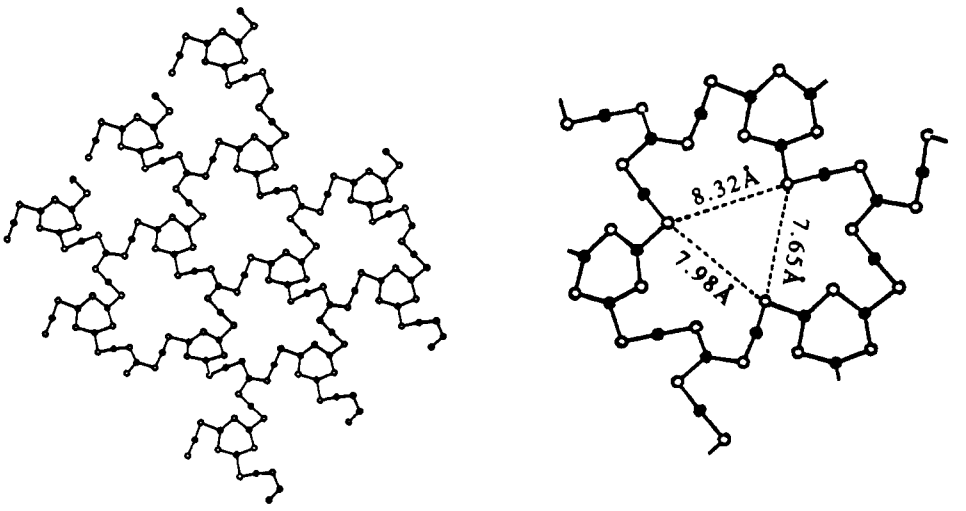

Figure 2. (A) Left: Two-dimensional structure of the $[Hg_7Se_9]_n^{4n-}$ anionic framework. (B) Right: View of a large hole itself with its dimensions. Filled circles represent Hg atoms.

structure. The reaction of $HgCl_2$ with Na_2Se in DMF solution in the presence of Et_4NBr followed by filtration and careful dilution with ether produced light yellow hexagonal platelets of $(Et_4N)_4[Hg_7Se_9]$ in 54% yield. A single-crystal X-ray diffraction study[7] surprisingly revealed that the crystals contain $[Hg_7Se_9]_n^{4-}$ (II), an anionic polymeric framework.

II possesses an unprecedented layered structure. Asymmetric units of II are combined together to form a 2-D framework structure, as shown in Figure 2. An intriguing feature in the structure is that the layers are perforated with large holes composed of 30-membered rings of alternating Hg and Se atoms, as shown in Figure 2A. One such large hole and its dimensions are shown in Figure 2B. These holes are large enough to be comparable to those typically found in zeolite and $AlPO_4$ structures, particularly those of $AlPO_4$-5[8] and VPI-5.[9] The layers are corrugated. The average distance between the layers is 8.03 Å. The Et_4N^+ organic countercations are located between layers, and some alkyl chains of these cations are penetrating into the large holes.

In the asymmetric unit of II (see Figure 3), there are three linearly coordinated and four trigonal-planarly coordinated Hg atoms. The average Hg–Se bond distances around linear and trigonal-planar Hg atoms are 2.43 (1) and 2.57 (8) Å, respectively. Another example of a mercury chalcogenide complex containing trigonal-planar Hg atoms was found in the polymeric $[Hg_2Te_5]_n^{2n-}$.[4]

Recently, a new family of metal–sulfide-based materials with open 3-D frameworks composed of antimony, germanium, or tin sulfide frameworks and tetraalkylammonium ions was reported.[10] Another example of a layered framework structure is found in $(NH_4)_2[PdS_{11}]\cdot 2H_2O$.[11] The stability of such materials suggests interesting possibilities for a next family of microporous substances, based on heavier chalcogenides. Even though 3-D microporous materials based on metal–chalcogenides have yet to be achieved, the pseudo-1-D structure of I and the perforated layered structure of II in combination with previous reports[10] suggest that it may be possible to get microporous 3-D framework structures by using appropriate templating organic cations.

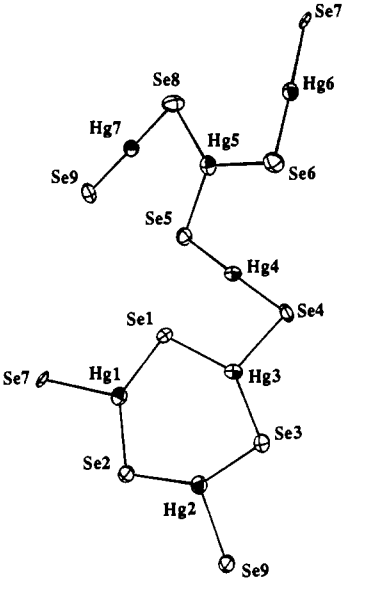

Figure 3. ORTEP representation and labeling scheme of the $[Hg_7Se_9]^{4-}$ asymmetric unit. Atoms Se(7) and Se(9) are repeated to help understand the connectivity of the units. Selected bond distances (Å) and angles (deg) are as follows: Hg(1)–Se(1), 2.510 (7); Hg(1)–Se(2), 2.537 (7); Hg(1)–Se(7), 2.666 (7); Hg(2)–Se(2), 2.479 (8); Hg(2)–Se(3), 2.542 (7); Hg(2)–Se(9), 2.685 (7); Hg(3)–Se(1) 2.527 (8); Hg(3)–Se(3), 2.493 (7); Hg(3)–Se(4), 2.700 (6); Hg(4)–Se(4) 2.431 (7); Hg(4)–Se(5), 2.456 (7); Hg(5)–Se(5), 2.568 (7); Hg(5)–Se(6), 2.556 (7); Hg(5)–Se(8), 2.538 (8); Hg(6)–Se(6), 2.424 (7); Hg(6)–Se(7), 2.425 (7); Hg(7)–Se(8), 2.427 (8); Hg(7)–Se(9), 2.422 (7); Se(1)–Hg(1)–Se(2), 137.1 (3); Se(1)–Hg(1)–Se(7), 116.1 (2); Se(2)–Hg(1)–Se(7), 106.7 (2); Se(2)–Hg(2)–Se(3), 140.4 (2); Se(2)–Hg(2)–Se(9), 115.4 (2); Se(3)–Hg(2)–Se(9), 104.2 (2); Se(1)–Hg(3)–Se(3), 139.9 (2); Se(1)–Hg(3)–Se(4), 102.4 (2); Se(3)–Hg(3)–Se(4), 117.4 (2); Se(4)–Hg(4)–Se(5), 174.7 (2); Se(5)–Hg(5)–Se(6), 114.0 (2); Se(5)–Hg(5)–Se(8), 122.6 (2); Se(6)–Hg(5)–Se(8), 123.4 (3); Se(6)–Hg(6)–Se(7), 178.7 (3); Se(8)–Hg(7)–Se(9), 173.7 (3).

In summary, the employment of shorter selenide ligands (Se_x^{2-}, $x = 1, 2$) has produced novel mercury–selenide complexes with structures intermediate between the molecular and the 3-D solid-state regime. Various organic cations of different size are being used with various Hg^{2+}:Se_x^{2-} ($x = 1, 2$) ratios to explore the templating ability of counterions for new framework structures.

(7) Crystal data for $(Et_4N)_4[Hg_7Se_9]$ (II): orthorhombic $Pna2_1$, $Z = 4$, $a = 16.066$ (5) Å, $b = 14.594$ (3) Å, $c = 24.754$ (7) Å, $V = 5804$ Å^3 at 166 K, and $2\theta_{max}$(Mo Kα) = 45°. Number of data measured: 4281. Number of data having $F_o^2 > 3\sigma(F_o^2)$: 2563. $D_{calc} = 3.02$ g/cm^3. Crystal dimensions: 0.09 × 0.22 × 0.31 mm. An empirical absorption correction was applied; $\mu = 241$ cm^{-1}. A decay of 9% was observed. A decay correction was applied. The correct enantiomorph gave final $R = 0.053$ and $R_w = 0.065$. All data were collected on a Nicolet P3F four-circle diffractometer.

(8) Wilson, S. T.; Lok, B. M.; Messina, C. A.; Cannan, T. R.; Flanigen, E. M. *J. Am. Chem. Soc.* **1982**, *104*, 1146–1147.
(9) Davies, M. E.; Saldarriaga, C.; Montes, C.; Garces, J.; Crowder, C. *Nature* **1988**, *331*, 698–699.
(10) (a) Bedard, R. L.; Wilson, S. T.; Vail, L. D.; Bennett, E. M.; Flanigen, E. M. *Zeolites: Facts, Figures, Future*; Jacobs, P. A., van Santen, R. A. Eds.; 1989; Elsevier Science Publishers B. V.: Amsterdam; pp 375–387. (b) Parise, J. B. *Science* **1991**, *251*, 293–294.
(11) Haraden, P. S.; Cronin, J. L.; Krause, K. A.; Katz, L. *Inorg. Chim. Acta* **1977**, *25*, 173–179.

Acknowledgment. Financial support from the donors of the Petroleum Research Fund, administered by the American Chemical Society, is gratefully acknowledged. We are grateful to the National Science Foundation for a Presidential Young Investigator Award. This work made use of the SEM facilities of the Center for Electron Optics at Michigan State University.

Supplementary Material Available: Tables of atomic coordinates of all atoms, anisotropic and isotropic thermal parameters of all non-hydrogen atoms, bond distances and angles, and calculated and observed powder patterns for I and II (21 pages); listings of calculated and observed ($10F_o/10F_c$) structure factors for I and II (68 pages). Ordering information is given on any current masthead page.

Department of Chemistry and Center for Fundamental Materials Research
Michigan State University
East Lansing, Michigan 48824

Kang-Woo Kim
Mercouri G. Kanatzidis*

Received December 26, 1990

Volatile Copper and Barium–Copper Alkoxides. Crystal Structure of a Tricoordinate Copper(II) Complex, $Ba\{Cu[OCMe(CF_3)_2]_3\}_2$

The recent discovery of ceramic superconductors has prompted considerable research into the development of new copper and barium precursors for sol-gel and chemical vapor deposition (CVD) processes.[1] This research has resulted in recent reports of a number of new alkoxides, siloxides, organometallics, and acetylacetonates.[2] The Buhro group synthesized the most volatile copper alkoxide reported to date, $Cu[OCHMeCH_2NMe_2]_2$ (sublimed at 60 °C).[2d] The most volatile barium source in common use is $Ba(FOD)_2$, which transports at 170–200 °C,[1] although more volatile organometallics (Cp^*_2Ba at 135 °C) are known.[2f] As bulky fluorinated ligands have allowed numerous volatile alkoxides of other metals to be synthesized,[3] we have recently been utilizing the hexafluoro-*tert*-butoxide [HFTB = $OCMe(CF_3)_2$] and perfluoro-*tert*-butoxide [PFTB = $OC(CF_3)_3$] ligands in our work. Thus we synthesized the structurally unique mixed alkoxide $Ba[Cu(HFTB)_3]_2$ (**1**), which is the first crystallographically characterized example of tricoordinate Cu(II). We have also prepared an extraordinarily volatile copper(II) perfluoro-*tert*-butoxide, tentatively identified as $Cu_4(PFTB)_7$ (**2**), and the corresponding Cu(I) complex,[4] $[Cu(PFTB)]_n$ (**3**). Compound **1** sublimed at 70–90 °C, **2** and its etherates transported under vacuum below room temperature, and **3** sublimed at 40–50 °C.[5a]

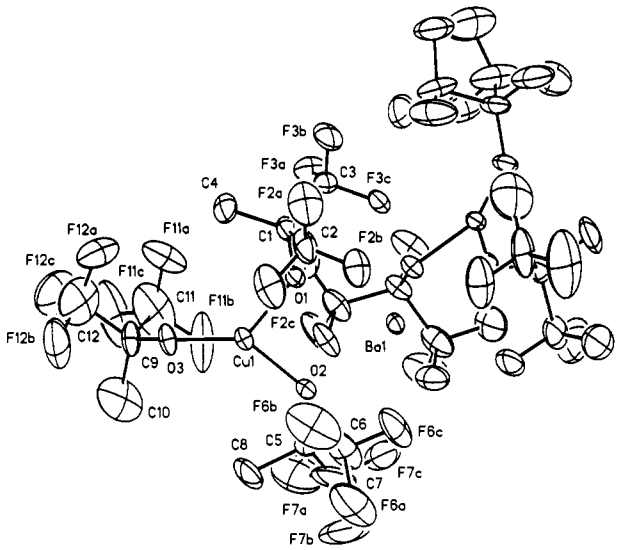

Figure 1. Plot of **1** drawn from experimental coordinates. Fluorines for the CF_3–CH_3 disorders at C(10) and all hydrogen atoms are not shown, and Ba coordination is omitted for clarity. Cu–O(1) = 1.889 (6) Å, Cu–O(2) = 1.878 (7) Å, Cu–O(3) = 1.781 (7) Å, ∠O(1)–Cu–O(2) = 88.4 (3)°, ∠O(2)–Cu–O(3) = 140.7 (3)°, and ∠O(1)–Cu–O(3) = 130.9 (3)°. Average C–C = 1.53 (2) Å, and average C–F = 1.33 (3) Å.

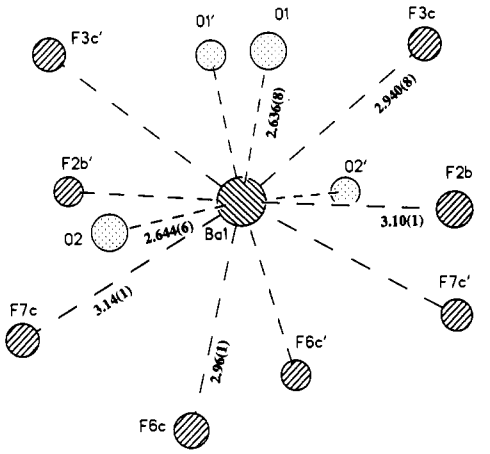

Figure 2. Environment of Ba, atoms labeled with a prime are related by the symmetry operation ($-x$, y, $^1/_2 - z$). Ba interacts with only two $Cu(OR)_3^-$ fragments. Ba--Cu = 3.612 (2) Å.

We believe **1**–**3** to be the most volatile copper and barium alkoxides known today.

The new barium alkoxycuprate $Ba[Cu(HFTB)_3]_2$ (**1**) was synthesized from a reaction between $Ba(HFTB)_2$ and $CuCl_2$. When the reactants were combined in a 1:1 mole ratio,[6b] a very

(1) For example: (a) Rupich, M. W.; Lagos, B.; Hachey, J. P. *Appl. Phys. Lett.* **1989**, 55, 2447. (b) Bradley, D. C. *Chem. Rev.* **1989**, *89*, 1317. (c) Mehrotra, R. C. *Mater. Res. Soc. Symp. Proc.* **1988**, *121*, 81. (d) Zhao, J.; Dahmen, K.; Marcy, H. O.; Tonge, L. M.; Marks, T. J.; Wessels, B. W.; Kannewurf, C. R. *Appl. Phys. Lett.* **1988**, *53*, 1750.

(2) (a) McMullen, A. H.; Tilley, T. D.; Rheingold, A. L.; Geib, S. J. *Inorg. Chem.* **1989**, *28*, 3772–4. (b) Goel, S. C.; Kramer, K. S.; Gibbons, P. C.; Buhro, W. E. *Inorg. Chem.* **1989**, *28*, 3619. (c) Horowitz, H. S.; McLain, S. J.; Sleight, A. W.; Druliner, J. D.; Gai P. L.; VanKavelaar, M. J.; Wagner, J. L.; Biggs, B. D.; Poon, S. J. *Science* **1989**, *243*, 66. (d) Goel, S. C.; Kramer, S. K.; Chaing, M. Y.; Buhro, W. E. *Polyhedron* **1990**, *9*, 611–613. (e) Hanusa, T. P. *Polyhedron* **1990**, *9*, 1345. (f) Burns, C. J.; Andersen, R. A. *J. Organomet. Chem.* **1987**, *325*, 31. (g) Sauer, N.; Garcia, E.; Salazar, K.; Ryan, R.; Martin, J. *J. Am. Chem. Soc.* **1990**, *112*, 1524. (h) Poncelet, O.; Hubert-Pfalzgraf, L. G.; Daran, J. C. *Inorg. Chem.* **1990**, *29*, 2883. (i) Purdy, A.; Berry, A. US Pat. 4982019, Jan 9, 1991.

(3) Willis, C. J. *Coord. Chem. Rev.* **1988**, *88*, 133–202.

(4) A mixture of MesCu (0.50 g, 2.74 mmol, Alfa Products), H(PFTB) (0.75 g, 3.18 mmol), and hexane (10 mL) was stirred at 60–70 °C for 1.5 h and then filtered to an orange solution and a brown residue. Solvent was removed at 0 °C; 0.39 g of sublimate was sublimed from the remaining solid at 60 °C, recrystallized from hexane, and dried in vacuo (0 °C), affording 0.19 g (23%) of the pale yellow **3**. Anal. Found (calcd) for C_4F_9OCu: C, 16.18 (16.09); H, 0 (0); F, 57.09 (57.27); Cu, 21.41 (21.28). Mp: 67–151 °C. NMR: ^{19}F δ −75.3.

(5) (a) Dynamic vacuum at $<10^{-5}$ Torr. (b) All manipulations were done under inert atmosphere. Proton and ^{19}F NMR were run at 300.13 and 282.4 MHz respectively. Electronic spectra were recorded from 1200 to 230 nm in hexane.

(6) (a) BaH_2 (1.13 g, 8.11 mmol) and H(HFTB) (2.5 mL) were stirred for 12 h in THF (5 mL) and filtered. $Ba(HFTB)_2$ (3.46 g, 85%) was isolated by solvent removal and drying at 100 °C in vacuo. Anal. Found (calcd): C, 19.22 (19.24); H. 1.29 (1.21); F, 45.43 (45.65). NMR (C_4D_8O): ^1H δ 1.35; ^{19}F δ −76.6. $Ba(PFTB)_2$ was prepared in a similar manner. (b) $Ba(HFTB)_2$ (0.67 g, 1.3 mmol), $CuCl_2$ (0.18 g, 1.3 mmol), and Et_2O (25 mL) were stirred at 70 °C for 1 day and filtered. After solvent removal from the filtrate at 0 °C, the residue was sublimed at 40–70 °C. Sublimation residue was recrystallized from C_6H_6/heptane affording **1** (0.16 g, 27%). A drop of unidentified orange liquid was distilled at room temperature from the heptane wash of the sublimate. (c) $Ba(HFTB)_2$ (0.502 g, 1.01 mmol), $CuCl_2$ (0.089 g, 0.66 mmol), and THF (8 mL) were stirred at 25 °C for 2 days and filtered, and solvent was removed from the filtrate to afford a solid (0.38 g. Anal. Found: C, 20.59; H, 1.23; Cu, 8.89; Ba, 13.21; Cl, 1.03; consistent with $Ba_2Cu_3(HFTB)_9Cl$). A 0.285-g sample of the latter was sublimed, affording **1** (0.14 g, 31%). A similar reaction in Et_2O (60–70 °C, 7 days), gave a 21% yield of **1**.

0020-1669/91/1330-1969$02.50/0 © 1991 American Chemical Society